IEEE Access
Multidisciplinary | Rapid Review | Open Access Journal

Received February 7, 2018, accepted March 5, 2018, date of publication March 14, 2018, date of current version April 4, 2018.

Digital Object Identifier 10.1109/ACCESS.2018.2815608

Restoration of Motion Blurred Images Based on Rich Edge Region Extraction Using a Gray-Level Co-Occurrence Matrix

MINGHUA ZHAO, XIN ZHANG, ZHENGHAO SHI, PENG LI, AND BING LI
School of Computer Science and Engineering, Xi'an University of Technology, Xi'an 710048, China

Corresponding author: Minghua Zhao (mh_zhao@126.com)

This work was supported in part by the National Natural Science Foundation of China under Grant 61401355, Grant 61472319, and Grant 61502382, in part by the Key Laboratory Foundation of Shaanxi Education Department, China, under Grant 14JS072, in part by the Science and Technology Project Foundation of Beilin District, Xi'an City, China, under Grant GX1621, and in part by the Science and Technology Project of Xi'an City under Grant 2017080CG/RC043(XALG011) and Grant 2017080CG/RC043(XALG021).

ABSTRACT To improve the efficiency of blur kernel estimation based on prior knowledge, a method of deblurring an image based on rich edge region extraction using a gray-level co-occurrence matrix is proposed in this paper. First, the relationship between the image edge information and the related coefficients of a gray-level co-occurrence matrix is analyzed, based on which an index representing the amount of image edge information is proposed. Next, high-frequency layer information is extracted from the blurred image to be processed with a bilinear interpolation method in the luminance channel. Subsequently, the high-frequency layer image is divided into nine regions, based on a sliding window, and the rich edge region index of each region is calculated; then, the region with the richest edge information is extracted. Finally, the extracted rich edge region, instead of the entire motion blurred image, is used to estimate the blur kernel with L0-regularized intensity and gradient prior, and the blurred image is blindly restored. An image quality evaluation function and the operation time are used to evaluate the performance of the proposed method. Experimental results show that the proposed method can improve the recovery efficiency while ensuring the recovery quality as well.

INDEX TERMS Image processing, image restoration, image quality, motion blurred image, gray-level co-occurrence matrix, rich edge region.

I. INTRODUCTION

Motion blur in images is a common phenomenon and the restoration of motion blurred images has always been a research hotspot in the computer vision field. The blind restoration of a single image has significant practical and research value [1], [2]. However, due to the lack of information, single image restoration is a difficult task [3], [4].

The restoration of a single blurred image is a serious ill posed problem, and the most practical solution is to use prior knowledge of the image [5]. Krishnan *et al.* [6] introduced a novel scale invariant image prior. The algorithm is applicable to different blur formation models and has achieved successful results. However, several shortcomings still exist. First, when the blurred image contains a rich tiny structure, this method is limited in the blur kernel estimation process. Second, the algorithm is not efficient enough because of the models' complexity and too many iterations in the kernel estimation process.

Assuming that the blur kernel and the clear image are sparse in the curvelet and framelet domains, respectively, Cai presented an approach to remove motion blurring from a single image by formulating the blind blurring model as a new joint optimization problem [7]. The method removed the ambiguity between the blur kernel and the clear image. However, it was very time consuming. Fergus *et al.* [8] proposed a blind motion- deblurring method using prior image knowledge. The method used a mixed Gaussian model to fit the heavy tail distribution of the natural image gradient, and estimated the blur kernel and clear image with a variational Bayesian algorithm. The algorithm improved the restoration effect to a great extent. However, the ringing effects were obvious and extensive computation was required. Shan *et al.* [9] proposed the idea of using a piecewise function to fit the distribution of the natural image gradient. The algorithm suppressed the ringing phenomenon; however, the computation was still extensive and the running speed was still slow.

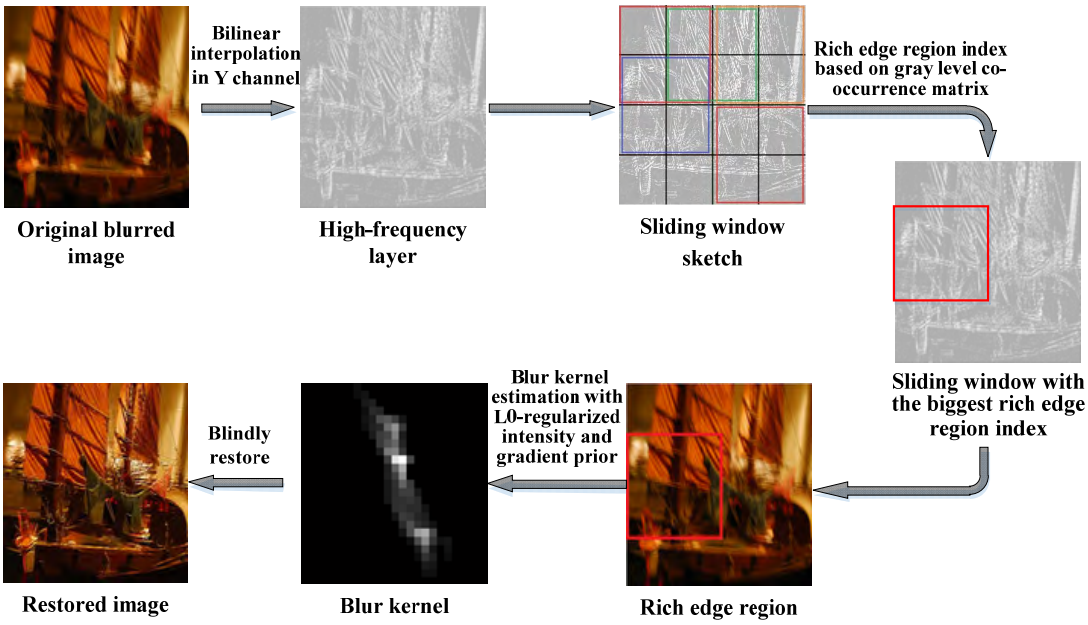

FIGURE 1. Framework of the proposed method.

Pan *et al.* [10] proposed an algorithm for deblurring text images via L0-regularized intensity and gradient prior. Using prior knowledge of the intensity and gradient, the method obtained a blur kernel based on recursive constraints and cleared the blurred text images. The prior knowledge can be used for kernel estimation of blurred text images, as well as natural blurred images. However, this restoration with prior knowledge is an iterative method and has high time complexity [11]. Cho and Lee [12] proposed a fast deblurring algorithm. In the blur kernel estimation process, the retained gradient value was greater than the threshold, and the optimization function was established using the image gradient. The algorithm's deblurring effect improved greatly; however, the recovery results were not always ideal, especially for images with rich details.

To improve the algorithm efficiency and guarantee the accuracy of the point spread function, it is possible to use a local image region instead of the entire blurred image to estimate the point spread function [13]. A new motion blurred image restoration method, based on rich edge region extraction using a gray-level co-occurrence matrix, is proposed in this paper, as shown in Figure 1.

First, an index representing the amount of image edge information is defined, based on the relationship between the image edge information and the related coefficients of the gray-level co-occurrence matrix [14], [15]. Next, high-frequency layer information is extracted from the blurred image with bilinear interpolation in the luminance channel. Subsequently, the high-frequency layer image is divided into nine regions based on a sliding window, and the rich edge region index of each region is calculated. Finally, the region with the richest edge information is extracted to estimate the blur kernel, and the blurred image is blindly restored.

II. EVALUATION CRITERION OF THE RICH EDGE REGION

A. GRAY-LEVEL CO-OCCURRENCE MATRIX

When estimating the motion kernel based on the L0-regularized intensity and gradient prior, the rich edge region is more likely to be affected by motion blur, and often contains more information that can improve the accuracy of the motion kernel. To improve the blurred image restoration efficiency, part of the image can be selected to estimate the blur kernel, instead of the entire image. The characteristics of the gray-level co-occurrence matrix can be used to automatically select the rich edge regions in the image.

A gray-level co-occurrence matrix can be obtained from the gray image, and its characteristics can be used to represent some image texture features. The inverse difference moment represents the local homogeneity of an image. A large inverse difference moment indicates that the image texture regions differ only slightly and the local homogeneity is very uniform. The moment of inertia, also known as the contrast ratio, measures the local change in an image and reveals the depth of the image's texture. A large moment of inertia indicates that the texture of a groove is deep.

A group of images with gradually increasing edge regions are shown in Figure 2. Equations (1) and (2) are used to calculate the sum of the inverse difference moment and the sum of the moment of inertia in the 0°, 45°, 90°, and 135° directions, respectively.

$$M_c = M_c^0 + M_c^{45} + M_c^{90} + M_c^{135} \tag{1}$$

$$M_d = M_d^0 + M_d^{45} + M_d^{90} + M_d^{135} \tag{2}$$

where M_c^θ and M_d^θ are the moment of inertia and the inverse difference moment in the θ direction, respectively.

Figure 3 shows the definition of the directions. A is the current pixel and A_i is the angle i degrees from A. The results are shown in Figure 4 and Figure 5. It can be seen from the two

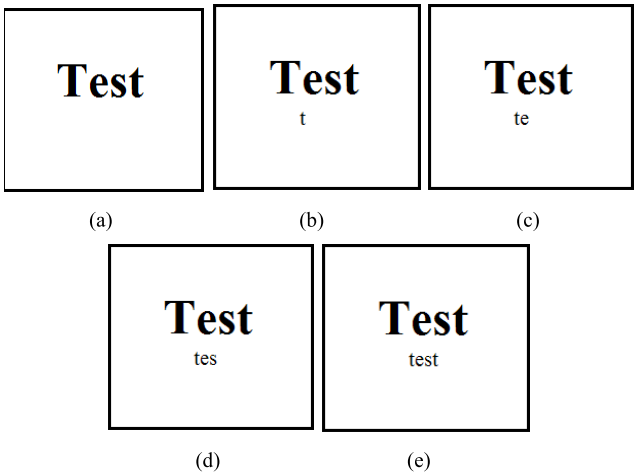

FIGURE 2. Images with incrementing edge information.

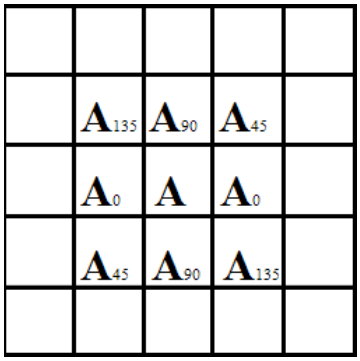

FIGURE 3. Direction definition.

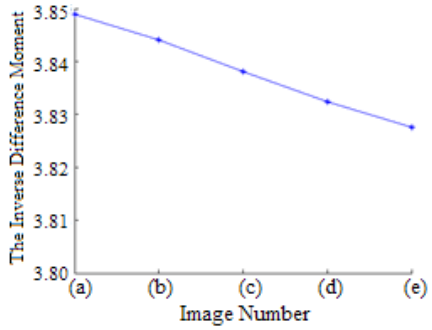

FIGURE 4. Inverse difference moments of Fig. 2 (a), (b), (c), (d), and (e).

figures that, with the increase of the image's edge, the value of the inverse difference moment decreases, while the value of the moment of inertia gradually increases.

B. INDEX OF RICH EDGE REGION

The index of the rich edge region is defined to evaluate the edge information of a single region, and is calculated as Equation (3).

$$R = M_c - M_d \tag{3}$$

where R is the rich edge index of an image and M_c and M_d are defined in Equations (1) and (2), respectively.

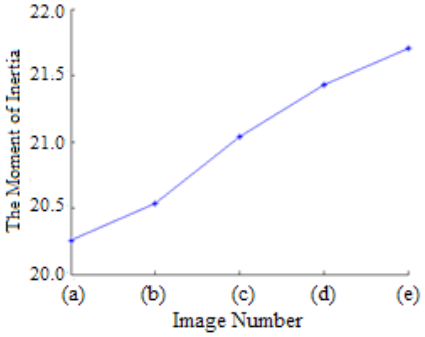

FIGURE 5. Moments of inertia of Fig. 2 (a), (b), (c), (d), and (e).

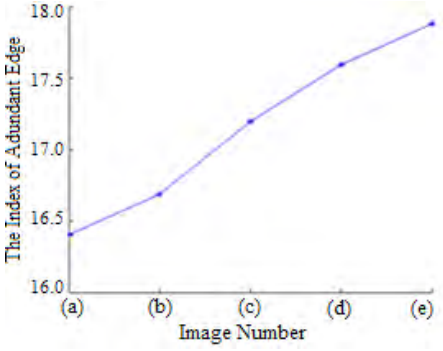

FIGURE 6. Rich edge region index of Fig. 2 (a), (b), (c), (d), and (e).

The rich edge index values of Figure 2 are shown in Figure 6. From Figure 6, we can see that the index values increase with the edge information. The index can be used to extract rich edge regions.

III. IMAGE RESTORATION BASED ON RICH EDGE REGION EXTRACTION

When using prior information to iteratively estimate the blur kernel, the high time complexity is an unavoidable problem. To improve the image restoration efficiency, it is possible to select part of the image instead of the entire image for the point spread function estimation. Image deblurring based on rich edge region extraction is composed of two main steps: Rich edge region extraction based on a gray-level co-occurrence matrix and the blur kernel estimation of the rich edge region.

A. RICH EDGE REGION EXTRACTION

The edges and details of an image are usually the regions with severe transformations and correspond to the high-frequency components in the frequency domain; the smooth parts of the image correspond to the low-frequency components. The high-frequency layer of a motion blurred image is extracted, using the following steps to obtain the rich edge regions.

Firstly, the original image is transformed from the RGB color space to the YCbCr color space, using Equation (4) to

extract the value of the Y channel.

$$\mathrm{Y} = 0.257 \times \mathrm{R} + 0.564 \times \mathrm{G} + 0.098 \times \mathrm{B} + 16 \quad (4)$$

where R, G, and B are the values of the three color channels, and Y is the luminance channel value.

Secondly, the Y channel is down-sampled by a factor of 2 and then bilinear interpolation is used to up-sample it by a factor of 2, which is shown as Equation (5).

$$Y' = B_2(Y(2:2:m, 2:2:n)) \quad (5)$$

where m and n are the row and column numbers of the original image, respectively, B_2 represents the bilinear interpolation of up-sampling by a factor of 2, and Y' represents the sampling result.

Thirdly, the luminance of the sampling result is subtracted from the luminance of the original image, and the high-frequency layer of the image is obtained, which is shown as Equation (6).

$$\mathrm{H} = \mathrm{Y} - Y' \quad (6)$$

where H is the high-frequency layer of the image.

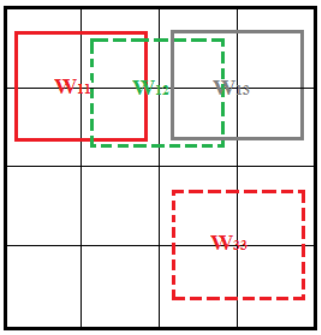

FIGURE 7. Sliding window of an image.

Fourthly, the high-frequency layer image is divided into nine regions, based on a sliding window, as shown in Figure 7. The rich edge region index of each region is calculated with Equation (3) and the blurred image region corresponding to the window with the largest rich edge index W is selected as the rich edge region, as shown in Equation (7).

$$\begin{aligned} \mathrm{W} &= \mathrm{MAX}(\mathrm{M}_c - \mathrm{M}_d) \\ &= \mathrm{MAX}\big(\mathrm{SUM}(\mathrm{M}_c^{\theta}(\mathrm{H}_{ij})) - \mathrm{SUM}(\mathrm{M}_d^{\theta}(\mathrm{H}_{ij}))\big) \\ &= \mathrm{MAX}\big(\mathrm{M}_c(\mathrm{H}_{ij}) - \mathrm{M}_d(\mathrm{H}_{ij})\big) \\ &= \mathrm{MAX}\big(\mathrm{R}(\mathrm{W}_{ij})\big) \\ &\quad (i = 1, 2, 3, j = 1, 2, 3, \theta = 0°, 45°, 90°, 135°) \end{aligned} \quad (7)$$

where i and j are the vertical and horizontal indices of the sliding window, respectively; W_{ij} is the blurred region covered by the sliding window, whose coordinate is (i, j) in the image; H_{ij} is the high-frequency layer information corresponding to the blurred area W_{ij}; MAX and SUM are the maximum and summation operations, respectively; $\mathrm{M}_c(\mathrm{H}_{ij})$ and $\mathrm{M}_d(\mathrm{H}_{ij})$ represent the moment of inertia and the inverse difference moment of the gray-level co-occurrence matrix H_{ij}; $\mathrm{R}(\mathrm{W}_{ij})$ is the rich edge index of blurred area W_{ij}; and W is the rich edge region extracted with the maximum rich edge index.

B. BLUR KERNEL ESTIMATION

Based on the extracted rich edge region, the L0-regularized intensity and gradient prior are used to estimate the blur kernel using an iterative method [16].

The prior of the image is defined as Equation (8).

$$\mathrm{P}(\mathrm{x}) = \sigma P_t(x) + P_t(\nabla x) \quad (8)$$

where $P_t(x)$ represents the number of pixels with nonzero values, $P_t(\nabla x)$ is the image gradient, and σ is a weight.

The prior P (x) is used as a regularization term to estimate the blur kernel of the blurred image with Equation (9).

$$\min_{\mathrm{x,k}} \|x * k - \mathrm{W}\|_2^2 + \gamma \|k\|_2^2 + \lambda P(x) \quad (9)$$

where W is the extracted rich edge region, x is the latent image of W in the blur kernel calculation process, k is a blur kernel, and γ and λ are weights.

The blur kernel is estimated from coarse to fine using Gaussian image pyramid. Once the blur kernel is obtained, the deblurring algorithm for shaken images proposed by Whyte *et al.* [17] is used to restore the motion blurred image.

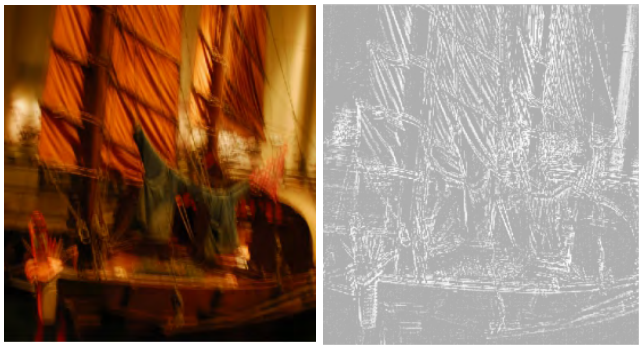

(a) (b)

FIGURE 8. High-frequency layer extraction (a) Blurred image (b) High-frequency layer.

IV. EXPERIMENTS AND ANALYSIS

A. EXTRACTION OF RICH EDGE REGION

Figure 8(a) is used to evaluate the proposed high-frequency information extraction performance, and the high-frequency layer extracted from Figure 8(a) is shown as Figure 8(b).

Two images from the internet, shown in Figure 9, are used to evaluate the rich edge region extraction performance of the proposed method. The length and width of the sliding window are initialized as half of the original image's length and width, and the sliding window is set to a quarter of the original blurred image size. The rich edge index for each sliding window area for Figure 9(a) and (b) is calculated with the proposed method, and the results are shown in Table 1.

(a) (b)

FIGURE 9. Extraction of rich edge region.

TABLE 1. Rich edge region index of each sliding window in Fig. 9.

Horizontal index \ Vertical index	i	1	2	3
	1	5.9741	8.8262	7.0975
Fig.9(a)	2	8.6004	11.2711	9.9038
	3	7.4211	9.0844	8.4517
	1	7.1751	13.0092	12.5921
Fig.9(b)	2	8.3407	11.6292	12.035
	3	5.7783	7.3361	7.2967

In Table 1, (i, j) is the sliding window coordinate, where i is the vertical index and j is the horizontal index. The regions with red rectangles in Figure 9 are the rich edge region extraction results. The rich edge indices of the red rectangle regions in Figures 9(a) and (b) are 11.2711 and 13.0092, respectively, which are larger than the other index values. From Figure 9, we can see that the red rectangle contains more edge information than the others, which accords with the rich edge region index.

B. VISUAL EVALUATION OF THE IMAGE RESTORATION RESULTS

The entire blurred image, the non-rich edge region, and the rich edge region are used to estimate the blur kernel and evaluate the image restoration performance. The original blurred images are shown in Figure 10(a). The rich edge region index of each sliding window is calculated, and the non-rich edge region and rich edge region are extracted respectively according to the smallest and largest indices. The L0-regularized intensity and gradient prior are used to estimate the blur kernel of the entire blurred image, the non-rich edge region, and the rich edge region. The restoration algorithm uses the estimated blur kernel to restore the blurred image. Figures 10 (b), (c), and (d) show the restoration results with blur kernel estimated using the entire image, the non-rich edge region, and the rich edge region and their corresponding enlarged views, respectively.

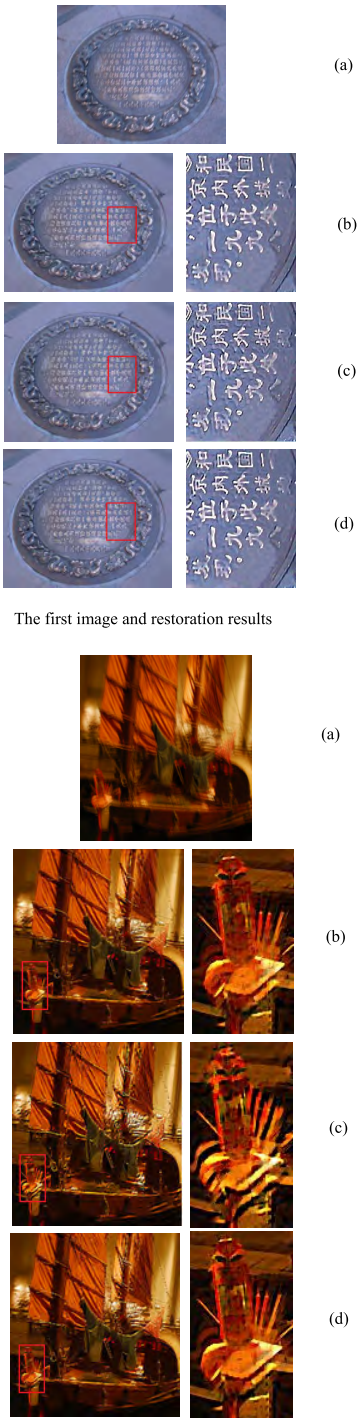

FIGURE 10. Blurred image and restoration results. (a) Blurred images. (b) Restoration results with blur kernel estimated using the entire image and the enlarged views. (c) Restoration results with blur kernel estimated using non-rich edge region and the enlarged views. (d) Restoration results with blur kernel estimated using rich edge region and the enlarged views.

Figure 10 reveals that blur kernel estimation using part of the image instead of the entire image can complete the restoration operation. The main reason is that a local image region can provide information, e.g., pixel intensity and gradient, to estimate the blur kernel. However, different local

regions contain different amounts of prior knowledge; thus, their restoration effects are different.

The recovery effect with the rich edge region is significantly better than that with the non-rich edge region. The main reason is that the rich edge region contains more information than the non-rich edge region about the pixel intensity and gradient, which are essential for blur kernel estimation. The restoration effect with the rich edge region is similar to that with the entire image, while the recovery time decreases significantly. This is mainly because the proposed method only needs part of the image in the blur kernel estimation process, which greatly reduces the calculation.

C. OBJECTIVE EVALUATION OF THE IMAGE RESTORATION RESULTS

The peak signal-to-noise ratio (PSNR), normalized mean square error (NMSE) [18], structural similarity (SSIM) [19], image quality index (Q) (shown as Equation (10)) [20], and recovery time are used to objectively evaluate the image restoration results [21].

$$Q = \frac{\sigma_{xy}}{\sigma_x \sigma_y} \cdot \frac{2\bar{x}\bar{y}}{(\bar{x})^2 + (\bar{y})^2} \cdot \frac{2\sigma_x \sigma_y}{\sigma_x^2 + \sigma_y^2} \tag{10}$$

where x and y represent the pixel values of the original image and the test image, respectively, and $\bar{x}$ and $\bar{y}$ are the average values of the pixels. σ_x^2, σ_y^2, and σ_{xy} are calculated using Equations (11), (12), and (13), respectively, where N is the number of pixels.

$$\sigma_x^2 = \frac{1}{N-1} \sum_{i=1}^{N} (x_i - \bar{x})^2 \tag{11}$$

$$\sigma_y^2 = \frac{1}{N-1} \sum_{i=1}^{N} (y_i - \bar{y})^2 \tag{12}$$

$$\sigma_{xy} = \frac{1}{N-1} \sum_{i=1}^{N} (x_i - \bar{x})(y_i - \bar{y}) \tag{13}$$

The restoration results for the first and second images of Figures 10 (b), (c), and (d) are shown in Tables 2 and 3, respectively. The blur kernel sizes of the first and second images in Figure 10(a) are 33×33 pixels and 25×25 pixels, respectively.

TABLE 2. Restoration quality for the first image in Fig. 10 (b), (c), and (d).

The first image in Fig. 10	(b)	(c)	(d)
Size/pixel	741x900	370x450	370x450
PSNR/dB	20.3236	19.5366	20.2048
NMSE	0.0373	0.0444	0.0383
Q	0.2474	0.2080	0.2698
SSIM	0.593	0.5276	0.6022
Time/s	891.97943	239.230114	239.283025

From Table 2 and 3, we can see that the image quality of the proposed method is slightly worse than the restoration result using the entire image for blur kernel estimation. However, its recovery time is about a quarter of that using the entire image. The recovery results with the rich edge region extracted by our proposed method are obviously better than those of the non-rich edge region; i.e., different local regions can provide different information. Regions containing rich edge information that is more conducive to blur kernel estimation can ensure the image quality and improve the recovery efficiency.

TABLE 3. Restoration quality for the second image in Fig. 10 (b), (c), and (d).

The second image in Fig.10	(b)	(c)	(d)
Size/pixel	613x568	306x284	306x284
PSNR/dB	20.2528	18.2534	20.1886
NMSE	0.091	0.1309	0.0903
Q	0.1978	0.2211	0.2777
SSIM	0.5535	0.5302	0.6012
Time/s	481.431666	112.208814	112.055218

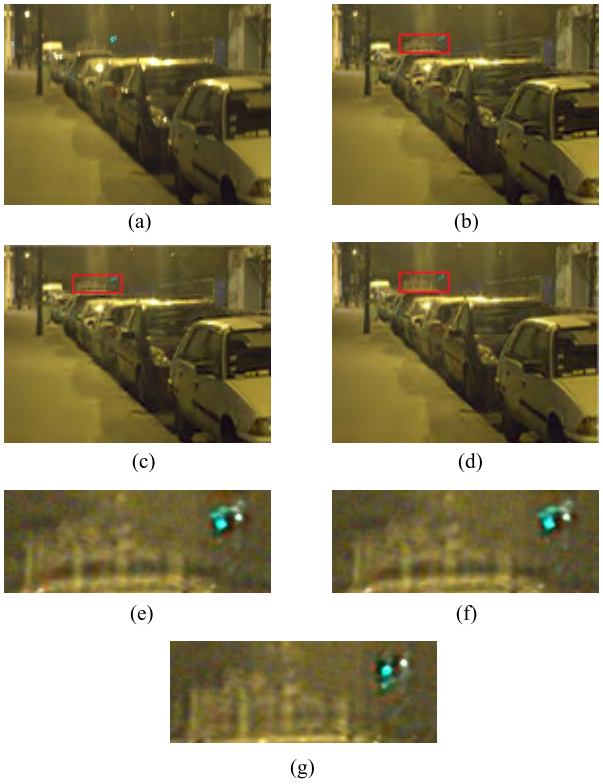

FIGURE 11. Effects of the rich edge region size on the restoration results. (a) Blurred image. (b) Restoration result with blur kernel estimated using the entire image. (c) Restoration result with blur kernel estimated using rich edge region with half of the image. (d) Restoration result with blur kernel estimated using rich edge region with a quarter of the image. (e) Enlarged view of the red-rectangle area in (b). (f) Enlarged view of the red-rectangle area in (c). (g) Enlarged view of the red-rectangle area in (d).

D. EFFECT OF THE RICH EDGE REGION SIZE ON THE RESULTS

Rich edge regions with different sizes are used to reveal the relationship between the size of the extracted rich edge region and the restoration effect. The restoration results with different sizes are shown in Figure 11. Figure 11(a) is the

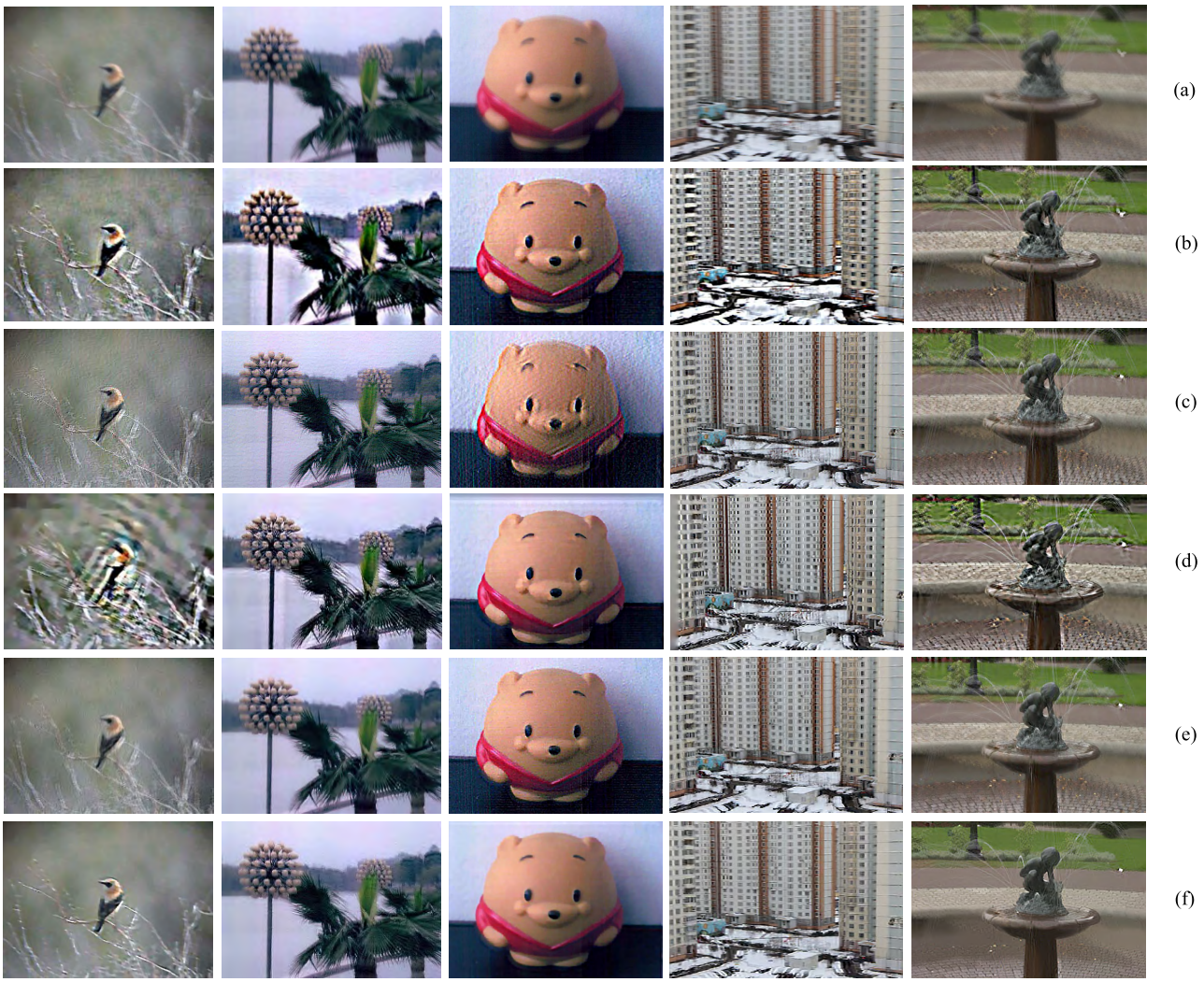

FIGURE 12. Visual comparison of the recovery results (a) Blurred image. (b) Krishnan [6]. (c) Shan [9]. (d) Zhong [20]. (e) Xu [21]. (f) Our method.

original blurred image; its kernel size is 53×53 pixels. Figures 11 (b), (c), and (d) are the restoration results using the entire image, half of the image, and a quarter of the image, respectively. The enlarged views of the red-rectangle regions in Figures 11 (b), (c), and (d) are shown as Figures 11 (e), (f), and (g), respectively. From Figure 11, we can see that the restoration effect improves with the increasing size of the rich edge region.

The assessment values of the restoration results with different sizes in Figure 11(a) are shown in Table 4. In Table 4, columns (b), (c), and (d) show the restoration results with blur kernel estimated using the entire image, half of the image, and a quarter of the image, respectively. Table 4 indicates when the rich edge region increases, the restoration effect improves and the recovery time increases; however, the recovery time is still far less than that using the entire image. The main reason is that a larger rich edge region can provide more related information.

TABLE 4. Restoration quality comparison for different rich edge region size.

Fig. 11	(b)	(c)	(d)
Size/pixel	767x1024	767x512	383x512
PSNR/dB	26.1615	26.5092	25.8997
NMSE	0.0172	0.0158	0.0183
Q	0.3287	0.3103	0.2501
SSIM	0.8031	0.8015	0.7876
Time/s	1549.940113	660.385243	446.270447

E. RESTORATION COMPARISON WITH OTHER METHODS

Blurred images from real scenes were used to compare the restoration results of our proposed method and other traditional methods. In Figure 12, row (a) shows the original blurred images, row (b) shows the restoration

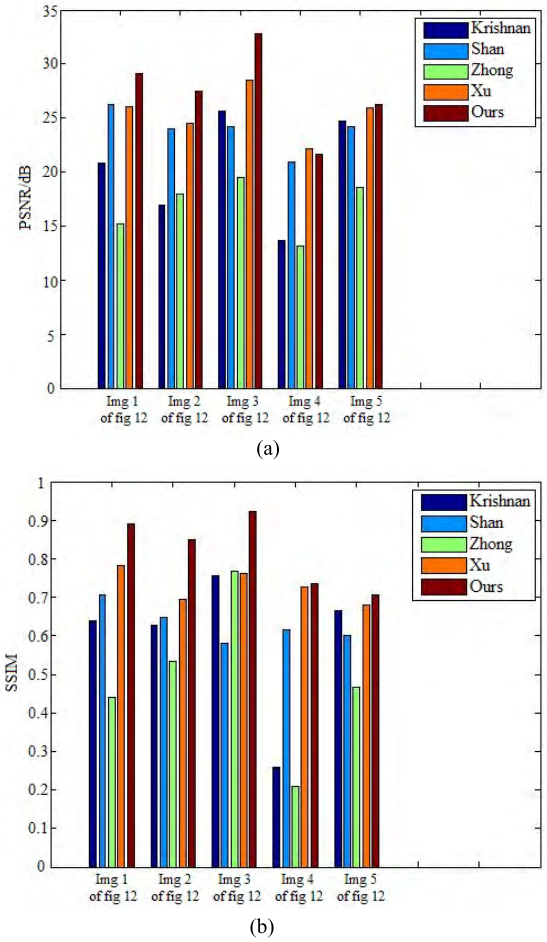

FIGURE 13. Objective comparison of the recovery results. (a) PSNR comparison. (b) SSIM comparison.

results with Krishnan's method [6], row (c) shows Shan's method [9], row (d) shows Zhong's method [4], row (e) shows Xu's method [22], and row (f) shows the restoration results with our proposed method. From Figure 12, we can see that the proposed method is better than the other four algorithms for blurred image restoration. The deblurred results of image 1, 2 and 4 contain area with unnatural color in row (b). The deblurred results of image 3 in row (c) appear obvious ringing effect. Ringing effect has also happened in the deblurred results of image 1, 4 and 5 in row (d). The motion blur is not fully removed for the results of image 1 in row (e). The PSNR values and SSIM values of the five methods are shown in Figure 13. We can see that the two values of the proposed method are mostly higher than those of the other four methods, which proves the effectiveness of the proposed method. The reason for the good deblurring performance of our proposed method is that the priors of the state-of-the-art methods are developed to exploit salient edges for motion deblurring and the low-frequency regions are ignored, while high-frequency information is used to extract abundant edge regions in our proposed method. What's more, the L0-regularized intensity prior is used to estimate the blur kernel in our proposed method, which is more effective for low frequency regions of the images in the deblurring process.

V. CONCLUSIONS

In this paper, an image deblurring method based on rich edge region extraction using a gray-level co-occurrence matrix was proposed. The method made three main contributions. First, the coefficients of the gray-level co-occurrence matrix were analyzed and an index representing the amount of image edge information was presented, which helped extract the rich edge region. Second, the high-frequency layer was extracted to compute the coefficients of the gray-level co-occurrence matrix. Third, a sliding window was used to divide the high-frequency layer image, and the rich edge region index of each region was calculated. The region with the richest edge information could replace the entire blurred image for blur kernel estimation and recovery. This greatly reduced the recovery time.

Experimental results, including the visual effect of the image restoration, calculation time, peak signal-to-noise ratio, normalized mean square error, structural similarity, and image quality index, showed that the proposed method was superior to the other methods in terms of recovery results. The proposed method not only effectively eliminated the motion blur of the image, but also improved the recovery efficiency to a certain extent.

However, the size of the rich edge region and the sliding interval of the sliding window were predefined. We will focus on automatically determining these two values in our future work.

REFERENCES

[1] A. Levin, Y. Weiss, F. Durand, and W. T. Freeman, "Understanding blind deconvolution algorithms," *IEEE Trans. Pattern Anal. Mach. Intell.*, vol. 33, no. 12, pp. 2354–2367, Dec. 2011.

[2] A. Levin, Y. Weiss, F. Durand, and W. T. Freeman, "Understanding and evaluating blind deconvolution algorithms," in *Proc. IEEE Conf. Comput. Vis. Pattern Recognit.*, Jun. 2009, vol. 8. no. 1, pp. 1964–1971.

[3] A. Gupta, N. Joshi, C. L. Zitnick, M. Cohen, and B. Curless, "Single image deblurring using motion density functions," in *Proc. Eur. Conf. Comput. Vis.*, vol. 6311. 2010, pp. 171–184.

[4] L. Zhong, S. Cho, D. Metaxas, S. Paris, and J. Wang, "Handling noise in single image deblurring using directional filters," in *Proc. IEEE Conf. Comput. Vis. Pattern Recognit.*, Jun. 2013, vol. 9. no. 4, pp. 612–619.

[5] L. Xu, S. Zheng, and J. Jia, "Unnatural L_0 sparse representation for natural image deblurring," in *Proc. IEEE Conf. Comput. Vis. Pattern Recognit.*, Jun. 2013, vol. 9. no. 4, pp. 1107–1114.

[6] D. Krishnan, T. Tay, and R. Fergus, "Blind deconvolution using a normalized sparsity measure," in *Proc. IEEE Conf. Comput. Vis. Pattern Recognit.*, Jun. 2011, vol. 42. no. 7, pp. 233–240.

[7] J.-F. Cai, H. Ji, C. Liu, and Z. Shen, "Blind motion deblurring from a single image using sparse approximation," in *Proc. IEEE Conf. Comput. Vis. Pattern Recognit.*, Jun. 2009, pp. 104–111.

[8] R. Fergus, B. Singh, A. Hertzmann, S. T. Roweis, and W. T. Freeman, "Removing camera shake from a single photograph," *ACM Trans. Graph.*, vol. 25, no. 3, pp. 787–794, 2006.

[9] Q. Shan, J. Jia, and A. Agarwala, "High-quality motion deblurring from a single image," *Acm Trans. Graph.*, vol. 27, no. 3, pp. 1–10, 2008.

[10] J. Pan, Z. Hu, Z. Su, and M.-H. Yang, "Deblurring text images via L_0-regularized intensity and gradient prior," in *Proc. IEEE Conf. Comput. Vis. Pattern Recognit.*, Jun. 2014, pp. 2901–2908.

[11] A. Beck and M. Teboulle, "A fast Iterative Shrinkage–Thresholding Algorithm with application to wavelet-based image deblurring," in *Proc. IEEE Int. Conf. Acoust.*, Apr. 2009, vol. 2. no. 1, pp. 693–696.

[12] S. Cho and S. Lee, "Fast motion deblurring," *ACM Trans. Graph.*, vol. 28, no. 5, pp. 89–97, 2009.
[13] W. Dong, G. Shi, and X. Li, "Nonlocal image restoration with bilateral variance estimation: A low-rank approach," *IEEE Trans. Image Process.*, vol. 22, no. 2, pp. 700–711, Feb. 2013.
[14] A. Levin, Y. Weiss, F. Durand, and W. T. Freeman, "Efficient marginal likelihood optimization in blind deconvolution," in *Proc. IEEE Conf. Comput. Vis. Pattern Recognit.*, Jun. 2011, vol. 42. no. 7, pp. 2657–2664.
[15] N. Joshi, R. Szeliski, and D. J. Kriegman, "PSF estimation using sharp edge prediction," in *Proc. IEEE Conf. Comput. Vis. Pattern Recognit.*, Jun. 2008, pp. 1–8.
[16] L. Xu, C. Lu, Y. Xu, and J. Jia, "Image smoothing via L_0 gradient minimization," *ACM Trans. Graph.*, vol. 30, no. 6, pp. 1–12, 2011.
[17] O. Whyte, J. Sivic, and A. Zisserman, "Deblurring shaken and partially saturated images," in *Proc. IEEE Int. Conf. Comput. Vis. Workshops*, 2012, vol. 110. no. 2, pp. 745–752.
[18] H. L. Tan, Z. Li, Y. H. Tan, S. Rahardja, and C. Yeo, "A perceptually relevant MSE-based image quality metric," *IEEE Trans. Image Process.*, vol. 22, no. 11, pp. 4447–4459, Nov. 2013.
[19] Z. Wang, A. C. Bovik, H. R. Sheikh, and E. P. Simoncelli, "Image quality assessment: From error visibility to structural similarity," *IEEE Trans. Image Process.*, vol. 13, no. 4, pp. 600–612, Apr. 2004.
[20] Z. Wang, H. R. Sheikh, and A. C. Bovik, "Objective video quality assessment," *Handbook Video Databases Des. Appl.*, vol. 17, no. 5, pp. 1041–1078, 2003.
[21] F. Gao, D. Tao, X. Gao, and X. Li, "Learning to rank for blind image quality assessment," *IEEE Trans. Neural Netw. Learn. Syst.*, vol. 26, no. 10, pp. 2275–2290, Oct. 2015.
[22] L. Xu and J. Jia, "Two-phase kernel estimation for robust motion deblurring," in *Proc. Eur. Conf. Comput. Vis.*, vol. 4. 2010, pp. 157–170.

MINGHUA ZHAO received the Ph.D. degree in computer science from Sichuan University, Chengdu, China, in 2006. She joined Xi'an University of Technology, Xi'an, China, where she is currently an Associate Professor with the School of Computer Science and Engineering. Her research interests include computer graphics, human-computer interaction, image processing, pattern recognition, and computer vision.

XIN ZHANG received the B.S. degree in computer science and technology from Xi'an University of Technology, Xi'an, China, in 2015, where she is currently pursuing the M.S. degree in computer science and technology. Her research interests include computer vision, image processing, and pattern recognition.

ZHENGHAO SHI received the Ph.D. degree in computer architecture from Xi'an Institute of Micro-electronics, Xi'an, China, in 2005. He joined Xi'an University of Technology, Xi'an, China, in 2000, where he is currently an Associate Professor with the School of Computer Science and Engineering. His research interests include image processing, pattern recognition, and computer-aided diagnosis.

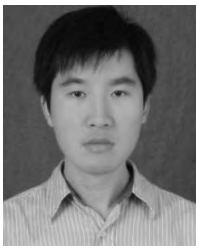

PENG LI received the M.S. degree in computer science and technology from Xidian University, China, in 2006. He joined Xi'an University of Technology, Xi'an, China, where he is currently a Lecturer with the School of Computer Science and Engineering. His research interests include computer architecture, image processing, and computer vision.

BING LI received the M.S. degree in computer science and applications from Xi'an University of Technology, China, in 2009. He joined Xi'an University of Technology, Xi'an, China, in 2000, where he is currently a Lecturer with the School of Computer Science and Engineering. His research interests include image processing, and computer vision, and artificial intelligence.